Strength and toughness of nanocrystalline SiO_2 stishovite toughened by fracture-induced amorphization

Kimiko Yoshida [a], Norimasa Nishiyama [b], Masato Sone [a], and Fumihiro Wakai [*a]

[a] Laboratory for Materials and Structures, Institute of Innovative Research, Tokyo Institute of Technology, R3-23 4259 Nagatsuta, Midori, Yokohama, 226-8503, Japan

[b] Deutsches Elektronen-Synchrotron (DESY), Notkestr. 85, 22607 Hamburg, Germany

Abstract

The finding of "fracture-induced amorphization" in nanocrystalline SiO_2 stishovite lead to a proposal of a new type of transformation toughening by the direct transition from crystal to amorphous state, which is different from the classical martensitic transformation of zirconia. Here, we investigated strength and toughness of nanocrystalline stishovite by using micro-cantilever beam specimens of different sizes. The maximum strength of 6.3 GPa gave the estimate of the lower bound of critical stress for amorphization, which was much higher than the critical transformation stress of zirconia. The crack growth resistance curve (R-curve) rose steeply with crack extension of only a few μm, and reached to a plateau value of 10.9 MPa $m^{1/2}$. We discussed the effects of grain size, microstrain, and dislocation density on the critical stress, the transformation zone width, and thereby, the fracture toughness.

Keywords: Ceramics; Fracture mechanisms; Nanocrystalline material;

Phase transformation;

* Author to whom correspondence should be addressed.

Tel.: +81-45-924-5361; fax: +81-45-924-5390.

E-mail address: wakai.f.aa@m.titech.ac.jp (F. Wakai)

1. Introduction

Silica (silicon dioxide, SiO_2) is a common mineral found in many rocks and sands. More than 90 % of the Earth's crust is composed of silicate minerals. Among them, quartz and silica glass are widely used because they are hard and transparent. However, they are brittle and easily broken. Stishovite is a high-pressure polymorph of silica stable at pressures above 9 GPa, and metastable at ambient conditions [1]. Stishovite has a denser structure than quartz, and has the highest hardness (33 GPa) of any stable/metastable oxide under ambient temperatures [2]. Hard materials with limited ability of plastic deformation tend to be brittle, then, the fracture toughness K_{IC} of a single crystal is 1.6 ± 0.3 MPa $m^{1/2}$ [3], which is not very high compared with that of silica glass (0.8 ± 0.3 MPa $m^{1/2}$) [4]. Recently, Nishiyama [5] found that a nanocrystalline SiO_2 stishovite with the grain size of ~100 nm had a fracture toughness of 13 ± 3 MPa $m^{1/2}$ by indentation fracture method (IF method [6]). This nanocrystalline material was synthesized by crystallization of silica glass at 15 GPa and 1473 K, in other words, the brittle glass is transformed to the novel advanced ceramics, which is tough and very hard, by the high-pressure synthesis.

At fixed synthesis pressure of 15 GPa, microstructures and mechanical properties of stishovite depend on the synthesis temperature. The average grain size increased with increasing the synthesis temperature. Williamson-Hall analysis revealed the

microstrain was 0.4 % in the sample synthesized at 1473 K, and decreased with increasing the synthesis temperature. TEM observation showed that dislocation density decreased with synthesis temperature. The fracture toughness also decreased with synthesis temperature, then, the fracture toughness of nanocrystalline stishovite increased with decreasing the grain size [5]. This effect of grain size on fracture toughness of stishovite is opposite to the behavior expected from the toughening mechanism by crack bridging [7], e.g., in alumina [8] and silicon nitride [7].

The fracture toughness of zirconia (ZrO_2)-based ceramics can be enhanced by martensitic transformation in the stress field of propagating cracks [9-11]. In analogy to the transformation toughening [12-14], Nishiyama [15] proposed a toughening mechanism by fracture-induced amorphization. Transformation of metastable stishovite with six-fold coordination to the stable phase with four-fold coordination often occurs through intermediate amorphous state, because the Gibbs free energy of stishovite is higher than that of amorphous SiO_2 at any temperature above 0 K at ambient pressure [16]. The direct transition of crystal to amorphous state, which is analogous to melting, is triggered by heating at 1 bar [17], or decompression at room temperature. Here, the term amorphization/vitrification is used below the glass transition temperature, and the term melting is used above it. The amorphization is induced by fracture since the tensile stress,

which is equivalent to negative pressure, can be very large at the crack tip. The formation of amorphous phase with the thickness of a few tens of nanometers was observed on the fracture surface by X-ray absorption near edge structure (XANES) spectroscopy. Furthermore, fracture toughness increased with the amount of amorphous silica near the fracture surface [15].

Brittle ceramics can be toughened by crack-tip shielding which reduces the stress intensity factor experienced at crack tip. This effect depends on crack size, then, crack growth resistance increases with crack extension [18, 19]. Yoshida et al. [20] developed a micro-mechanical test method using micro-cantilever beam specimens to determine the very early part of resistance curve (R-curve) of nanocrystalline stishovite, and showed that crack growth resistance increased from 4 MPa $m^{1/2}$ to 8 MPa $m^{1/2}$ with crack extension of only one micrometer. The effect of toughening mechanism is described by a stress intensity change ΔK between the applied stress intensity factor and the stress intensity factor at the crack tip, which is assumed to be equal to the intrinsic toughness K_0. In the transformation toughening, the extent of ΔK is given by [13]

$$\Delta K = 0.22 \frac{E}{1-\nu} V_f \varepsilon^T \sqrt{h} \qquad (1)$$

where E is Young's modulus, ν is Poisson's ratio, V_f is the volume fraction of transformed phase in the transformation zone, ε^T is the dilatational strain accompanying transformation, and h is the transformation zone width. From Eq. (1), fracture resistance can be

increased significantly by the amorphous layer with the thickness of 10–50 nm, because the volumetric strain associated with the amorphization of stishovite is from 60 to 90 %, which is much larger than that in the tetragonal to monoclinic transformation of zirconia (4 %). The effect of crack shielding ΔK increases with crack extention Δa, and saturates to Eq. (1) at a certain crack length $\Delta a^* \approx 10h$ [12]. The sharply rising R-curve is the result of very narrow transformation zone width of nanocrystalline stishovite. Materials with rising R-curve lead to an increase in the strength, in many cases, the steeper the initial R-curve, the higher the strength [21].

The objective of the present paper is to study strength and toughness of nanocrystalline stishovite, so as to clarify the effect of microstrain on R-curve behavior. We used a large micro-cantilever beam specimen to study how R-curve rises and attains to a steady-state (plateau) value. We show the crack growth resistance reaches to more than 11 MPa $m^{1/2}$ with crack extension around 8 μm. The lower bound of the critical stress for amorphization is also discussed from the fracture strength.

2. Experimental procedure

2.1. Materials

Nanocrystalline stishovite sample was synthesized by a Kawai-type multi anvil high pressure apparatus (LPR 1000-400/50, Max Voggenreiter GmbH, Germany). The starting material was pure bulk

silica glass, whose dimension was 2.5 mm in diameter and 0.6 mm in height. All the impurities were less than 0.1 ppm except OH (about 800 ppm). The pure bulk silica glass was heated rapidly from 723 K to 1473 K under high pressure, 15 GPa. After holding at 1473 K either for 0.5 h or 5 h, temperature was decreased to 723 K, and decompression was started [5]. The average grain size of sample was determined by TEM observation, and microstrain was evaluated by X-ray diffraction pattern using Williamson-Hall method [22].

3 mol% Y_2O_3-stabilized tetragonal zirconia polycrystals (3Y-TZP) and alumina (Al_2O_3) samples were sintered using a spark plasma sintering machine (SPS-515S, Fuji Electronic Industrial). The temperature was measured by a radiation thermometers at surface of a graphite die. 3Y-TZP sample was sintered from commercial zirconia powders stabilized with 3 mol% Y_2O_3 (TZ3Y, Tosoh Co. Ltd., Japan). As-received powder was heated directly to 1673 K under a uniaxial pressure of 50 MPa. The heating rate was 50 K/min to sintering temperature, and holding 5 min at the temperature. Alumina sample was sintered from commercial α-alumina powder (TM-DAR, Taimei Chemicals Co. Ltd., Japan). As-received powder was heated under a uniaxial pressure of 80 MPa. The heating rate was 25 K/min from 873 K to 1273 K, and 8 K/min to 1423 K. After holding for 20 min at the sintering temperature, sample was annealed at 1273 K for 10 min in order to reduce the residual stress [23].

2.2. Fabrication of micro-cantilever beam specimens

The micro-cantilever beam specimens (Fig.1 (a)) was machined by a focused ion beam (FIB) machining (HITACHI-FB2100) using a high current Ga ion beam (40 keV, 32 nA), followed by fine machining at low currents (6 nA). A notch was introduced by using an even finer current beam (300 pA) in the direction perpendicular to the notch length, so that the contamination of Ga ion at the notch root is minimized (Fig.1 (b)). The notch-tip radius was 50 nm (Fig. 1 (c)). The side-grooves were cut to guide the crack (Fig. 1 (d)). The position-marks are made on the top surface and the side surface of the micro-cantilever beam specimens for easy positioning of the indenter (Fig. 1 (a)). All beam directions in the FIB machining are illustrated in Fig. 1 (e).

The thickness of surface layer damaged by ion beam was estimated by Monte Carlo simulation. When the 40 keV Ga ion beam hitting the stishovite target at a grazing angle of 89 degree, the thickness of damage was less than 20 nm. In this study, the specimen size was large enough, so that the influence of the ion beam machining can be neglected.

2.3. Micro-sized bending test

Micro-sized bending test were carried out in air using a mechanical testing machine designed for micro-sized specimen. The basic concept of this machine is described in [24]. The displacement was applied by a piezoelectric device at a displacement rate of 10-50 nm/sec. The load was applied by using a

spherical diamond indenter with radius of 2.5 μm. Load and displacement data were acquired with the sampling interval of 0.1 second.

2.4. Calculation of stress intensity factor and specimen compliance

The stress intensity factor (mode I) K_I of a notched micro-cantilever beam specimen was calculated by the extended finite element method (XFEM) using the commercial solver Abaqus 6.13 [20]. The stress intensity factors were determined by path-independent contour integral. Three-dimensional isotropic elastic model was employed to simulate the cantilever beam specimens with side grooves. The ratio K_{II}/K_I was less than 5 %.

The stress intensity factor of cantilever beam specimen with side-grooves was calculated, and expressed in the following equation

$$K_I = \frac{PL}{\sqrt{BB_N}W^{\frac{3}{2}}} f(a/W) \qquad (2)$$

where P is the applied force, L is the distance between the notch and the loading point, a is the crack length, W is the cantilever width, B is the thickness, and B_N is the minimum thickness measured at the root of the side grooves. The dimensionless shape factor can be used in the range $0.2 \le a/W \le 0.7$ for the cantilever beam specimens with side grooves ($H:L:W:B$ = 1:3:1:1, $B_N = 0.8B$), where H is the distance between the notch and the root of the cantilever beam

$$f\left(\frac{a}{W}\right) = 2.2996 + 7.6061\left(\frac{a}{W}\right) + 61.404\left(\frac{a}{W}\right)^2 - 193.33\left(\frac{a}{W}\right)^3 + 229.22\left(\frac{a}{W}\right)^4 . \quad (3)$$

The compliance $C \equiv u/P$ is expressed as

$$C = \frac{8}{E'\sqrt{BB_N}}\left(\frac{L}{W}\right)^2 f_C\left(\frac{a}{W}\right) \quad (4)$$

$$E' = \frac{E}{1-\nu^2} \quad (5)$$

where ν is Poisson's ratio. The dimensionless shape factor for the compliance f_c is given as

$$f_C\left(\frac{a}{W}\right) = 2.3235 + \frac{0.211}{(1-a/W)} + \frac{2.0172}{(1-a/W)^2} \quad . \quad (6)$$

The crack length is expressed as a function of $b = 1/\sqrt{f_C}$

$$\frac{a}{W} = 0.8866 + 0.9826b - 18.357b^2 + 56.933b^3 - 68.099b^4 . \quad (7)$$

The micro-sized bending test is carried out by controlling the displacement u' of the actuator

$$u' = u + C_{machine}P \quad (8)$$

where u is the displacement of the specimen, and $C_{machine}$ is the machine compliance. The machine compliance was 0.023 μm/mN. The initial compliance C_{ini} of notched specimen was obtained from the measured displacement ($u = CP$) and load. The theoretical compliance C_{calc} of the notched specimen was calculated by Eqs. (4) and (5) using specimen dimensions, Young's modulus of 531 ± 9 GPa, and Poisson's ratio of 0.21 ± 0.01 [Supplementary data of [5]]. The difference between C_{ini} and C_{calc} was within ± 5 %. The compliance measured from the load-displacement curve was calibrated by the

ratio C_{calc}/C_{ini}. The value of f_c was obtained by substituting the calibrated compliance to Eq. (4), then, the crack length was determined by Eq.(7). For the initial notch length of $a_0/W = 0.5$, data were taken at the crack extension of $\Delta a/W = 0.15$ to construct R-curves in most cases.

2.5. Calculation of fracture strength

The fracture strength of micro-cantilever beam specimens without notch were defined as a maximum flexural stress located on the tensile side of fixed end. According to the simple Euler-Bernoulli beam theory, it is

$$\sigma = \frac{6PL'}{BW^2} \tag{9}$$

where L' is the distance between the fixed end and the loading point. Three types of specimens with width W of 5, 20, 60 mm were used to study the effect of specimen size on the fracture strength. All specimen had self-similar shape: $B = W$ and $L' = 4W$.

2.6. Effect of side-groove on R-curve testing

The straight crack propagation is necessary to analyze the stress intensity factor by using the compliance method. Fig.2 shows the fractured micro-cantilever beam specimens with and without side grooves. The fracture surface of the specimen without side groove curved toward the fixed end. On the other hand, the crack propagated along side-grooves in the specimen with side groove

depth of 20 % ($B_N = 0.8B$), and the fracture surface was macroscopically flat. In this study, we used side-grooved specimens with 20% depth. Furthermore, side-grooves enhance plane strain fracture, i.e., the situation where the crack front remains straight as it extends [25, 26].

3. Results

3.1. Microstructure of nanocrystalline stishovite

Two nanocrystalline stishovite samples are prepared at 15 GPa and at 1473 K by holding either for 0.5 h or 5 h, which are designated as 0.5h sample and 5h sample, respectively. The microstructure were observed by transmission electron microscopy (TEM) (Fig.3). The average grain size of 0.5h sample was 128 ± 59 nm, and that of 5h sample was 164 ± 58 nm. TEM micrographs show complex contrast suggesting the presence of microstrain in these two samples.

The microstrain was determined by Williamson-Hall method, and plotted as a function of synthesis temperature in Fig. 4. Nishiyama et al. [5] showed that microstrain decreased with increasing synthesis temperature. The present data showed similar trend. At the synthesis temperature of 1473 K, calculated microstrain was 0.34 % and 0.24 % for 0.5h sample and 5h sample, respectively. The microstrain decreased 29 % with increasing the holding time, while grain size increased 28 %. The grain size and microstrain were almost the same with the sample synthesized at 1873 K for 0.5 h by

Nishiyama [Supplementary data of [5]]. However, the sample synthesized at 1873 K showed heterogeneous microstructure due to abnormal grain growth. In the present study, we compare mechanical properties of 0.5h sample and 5h sample, both of which have uniform microstructure.

3.2. R-curve of nanocrystalline stishovite

Fig. 5 (a) shows load (P)-displacement (u) curves of 0.5h sample measured by using notched specimens of different sizes. The dimensions of specimens are summarized in Table 1. All specimens showed stable fracture, and the occurrence of unstable fracture was indicated by the "X" mark. An arrow at the P-u curve of the largest specimen (W = 60 μm) also shows an unstable fracture. The R-curves were calculated by the compliance method from P- u curves of stable fracture before "X" mark, and plotted in Fig. 5 (b). While P- u curves depend on the specimen size and the notch length, R-curves were similar in shape for all specimens. The crack growth resistance rose steeply from 4 MPa $m^{1/2}$ to 8 MPa $m^{1/2}$ with crack extension of only a few μm, and reached to a plateau value of 10.9 MPa $m^{1/2}$. This value was comparable to the fracture toughness (13 MPa $m^{1/2}$) reported by Nishiyama [5].

Unstable fracture occurs when the following conditions are fulfilled [21]

$$K_I = K_R \tag{10}$$

$$\frac{dK_I}{da} = \frac{dK_R}{da}. \tag{11}$$

Stable fracture occurs at the beginning thanks to the very steep R-curve of nanocrystalline stishovite. Since dK_R/da decreases to zero as the crack extends to the plateau region, unstable fracture occurs at a critical crack length. For a given a/W and K_I, Eq. (2) predicts that dK_I/da decreases with increasing the specimen size. Then, from Eq. (11), the region of stable crack growth is extended by using larger specimens. As shown in Fig. 5 (b), we could observe R-curve behavior at crack extensions close to the plateau region.

Fig.6 shows the comparison between R-curves of the 0.5h sample and that of the 5h sample. For both materials the early part of the R-curves was relatively insensitive to specimen size. The initial R-curve was steeper in 0.5h sample with microstrain of 0.34 % than in the 5h sample with microstrain of 0.24 %. The plateau value of the 5h sample was 9.9 MPa $m^{1/2}$ which was 1 MPa $m^{1/2}$ lower than that of the 0.5h sample.

The fracture toughness was also measured by the indentation fracture method (IF method [6]) with 30, 20 and 10 kg loads. We used scanning electron microscopy to measure crack length precisely for comparison between 0.5h material and 5h material. The fracture toughness was 8.9 ± 0.40 MPa $m^{1/2}$ and 8.0 ± 0.49 MPa $m^{1/2}$ for 0.5h sample and 5h sample, respectively. The average fracture toughness of 0.5h sample was higher than that of 5h sample, although the difference was small. The crack length was also measured by optical microscope and CCD camera. The values of fracture toughness measured by optical microscopy agreed with previous report [15],

and was about 1 MPa $m^{1/2}$ higher than that measured by scanning electron microscopy.

3.3. Strength of nano-crystalline stishovite

The fracture strengths of nanocrystalline stishovite, 3Y-TZP, and alumina were measured by bending micro-cantilever beam specimens without notch. The nanocrystalline stishovite specimens showed brittle fracture. The load-displacement curves had no yield point until fracture. Measured strengths are plotted as a function of specimen volume in Fig.7 together with the data of single-crystal [25-27] and polycrystalline [28] silicon measured by micro-sized test. The volume of a cantilever specimen was defined as $V = BWL'$. The strength increased with decreasing the size of specimens. This size effect can be explained by Weibull theory for brittle fracture where the strength is controlled by the defect [29]. When fracture occurs from defects inside the specimen, and the Weibull modulus m is assumed to be constant, the strength increases with decreasing the effective volume V_E, which is proportional to the specimen volume V as long as specimens of self-similar shape are used

$$\sigma_f \propto (1/V_E)^{1/m} \quad . \tag{12}$$

The slopes of the lines fitted to the data of polycrystalline silicon gave the Weibull modulus of 5.7, which was smaller than the measured *m*-value of 7.5. The plots of stishovite data suggests that the Weibull modulus is larger than that of polycrystalline silicon.

For a fixed specimen volume of 20×20×80 = 32000 μm^3, the strength of nanocrystalline stishovite was higher than that of 3Y-TZP, alumina, and silica glass. The highest strength was 6.3 GPa and 6.1 GPa for the 0.5h sample and the 5h sample, respectively. The strength of the 0.5h sample was higher than that of the 5h sample, which may be explained by its steeper initial R-curve [21]. The present results also emphasize Kruzic et al.'s notion [30] that factors which contribute to the early part of the R-curve are critical for attaining both high strength and high toughness.

4. Discussion

4.1. Critical stress for amorphization

When the strength is limited by pre-existing flaw size, the strength is proportional to fracture toughness K_{IC} through the Griffith relation

$$\sigma_f = YK_{IC}/\sqrt{c} \qquad (13)$$

where Y is a geometry parameter and c is the flaw size. In the transformation toughening, crack-tip transformation occurs when the local stress reaches a critical stress σ_c. The transformation zone width h depends on the critical stress [13]

$$h \propto (K_I/\sigma_c)^2 . \qquad (14)$$

From Eq. (1) and Eq. (14), the fracture toughness increases as σ_c decreases ($\Delta K \propto V_f \varepsilon^T / \sigma_c$), then from Eq. (13), the strength increases with decreasing σ_c as illustrated in Fig. 8. However, as the

critical stress decreases further, the strength is limited by the critical stress to induce the phase transformation [13, 31]. In this region, the critical stress can be directly measured as the point of departure of stress-strain curves from linearity. It is 600 MPa for partially stabilized zirconia (Mg-PSZ), and 1.3 GPa for 2Y-TZP [31]. Camposilvan [32] recently observed transformation induced plasticity at 3 GPa in micro-cantilever test of 3Y-TZP. However, no plastic deformation was observed for 3Y-TZP and nanocrystalline stishovite in the present study. From Fig. 8, the strength in failure from pre-existing flaw gives the lower bound of the critical stress. The maximum strength of nanocrystalline stishovite was 6.7 GPa, so that the critical stress for amorphization must be larger than 7 GPa.

As well as stishovite, dense high pressure crystalline silicates such as $CaSiO_3$ and $MgSiO_3$ perovskite, where silicon is in octahedral coordination, transform under tension to a low-density glass composed of tetrahedral silicon. The molecular dynamic simulation revealed that high-pressure phases of $CaSiO_3$ and $MgSiO_3$ started amorphization at tensile stress of 18 GPa at 300K [33]. The absolute value of critical stress was close to Vickers hardness of $MgSiO_3$ (18 GPa) [34]. This result suggests that the upper bound of critical stress of stishovite is close to its hardness, 30 GPa, which is more than 10 times higher than the critical stress of zirconia. Substituting the critical stress of 30 GPa to Eq. (14), the transformation zone width of stishovite is estimated to be a

few tens of nanometers, much narrower than that of zirconia. This estimate agrees with the experimental observation by the surface-sensitive Si-K XANES measurement [15].

4.2. Origin of the critical stress

The transformation of metastable stishovite to the intermediate amorphous state is schematically illustrated by an energy diagram in Fig.9. The Gibbs free energy of stishovite is higher than that of amorphous SiO_2 at any temperature above 0 K [16]. However, there is an energy barrier between stishovite and amorphous state, and this barrier prevents the amorphization of stishovite at ambient condition. Stishovite transforms into the amorphous state during heating (890-950 K) at atmospheric pressure [17, 35]. Brazhkin [36] measured the phase transition of stishovite with the average grain size 10-40 μm by the annealing method, and reported the heat release Q of 41 ± 3 kJ/mol, the activation energy ΔG of 220-280 kJ/mol, and Avrami index n of 1. In the classical theory of nucleation, the amorphous nucleus forms within stishovite, and it grows with time. The value of Avrami index suggests that the rate controlling step of amorphization is the nucleation process. The energy of the nucleus formation is determined by the difference between the free energies of two phases, the energy connected with strain energy, and the interface energy of the nucleus. The observed activation energy was much lower than the theoretical prediction, hence Brazhkin [36] assumed heterogeneous nucleation

from defects.

The amorphization of stishovite is induced by tensile stress at crack tip during fracture also [15]. The thermodynamics of transformation under applied stress can be treated based on the original Patel and Cohen [37] criteria for stress-induced martensite transformation. Here, we consider only the dilatational strain ε^T in the amorphization. The work per unit volume done by an applied stress assisting the transformation is expressed by

$$W = \sigma\varepsilon^T . \quad (15)$$

For σ = 1 GPa and ε^T = 0.6, the work is 6 X 10^8 J/m^3, then, the driving force contribution of applied stress $\partial\Delta G/\partial\sigma$ is -8.41 kJ/mol/GPa. The driving force necessary for initiating the transformation is reduced by the application of tensile stress, for example, -250 kJ/mol at 30 GPa. The fracture-induced amorphization occurs at a critical tensile stress, which lowers the energy barrier.

4.3. Effects of grain size, microstrain, and dislocation on fracture toughness

The fracture-induced amorphization occurs in nanocrystalline materials with very small grain size, large microstrain, and high dislocation density. The sites of heterogeneous nucleation of amorphous phase can be defects including point defects, dislocations, and grain boundaries. The formation energy of nucleus is assumed to be reduced by the strain energy of a dislocation and

the grain boundary energy. It is supposed that the critical stress for nucleation decreases with decreasing the grain size and with increasing the dislocation density. Luo [38, 39] conducted molecular dynamic simulations to investigate the role of defects in amorphization of stishovite upon heating. The amorphization of stishovite required sufficient concentration of defects, 100 vacancies in 720 SiO_2 super cell [39]. Since the density of nanocrystalline stishovite (4.28 g/cm^3) [supplementary data of [5]] is almost the same with an X-ray density [40], the concentration of point defects is not enough to facilitate the amorphization. Molecular dynamic simulation showed also the spontaneous amorphization or disordering occurred in nanocrystalline stishovite when the grain size was less than 5 nm [38]. The formation of amorphous phase was observed only on transgranular fracture surface of nanocrystalline stishovite by using XANES, but, it was not detected on the intergranular fracture surface of a material with grain size of 30 μm [15]. Thus, we conclude that grain boundary is not the primary site of amorphization.

Nishiyama [5] observed many dislocations in the nanocrystalline stishovite. Cordier and Sharp [41] also showed the dislocation densities could locally reach values of 1 - 5 × 10^{13} m^{-2} in a stishovite consisted of grains ranging from 0.5 to a few micrometers, which was synthesized at 15 GPa and 1473 K. The dislocations observed in stishovite are thought to be derived by local deformation occurred during the synthesis of stishovite from

glass as a result of the large volume reduction [41]. The average microstrain of 0.24-0.34 % in the nanocrystalline materials corresponds to the internal stress of 1.3-1.7 GPa using Young's modulus of stishovite. The local tensile stress, which can be much larger than the average internal stress, would lower the critical stress for the nucleation of amorphous phase.

Fig.8 shows fracture strength increases with decreasing the critical transformation stress in the region where the failure occurs from pre-existing flaw. If the microstrains in nano-crystalline stishovite decrease the critical stress, it is reasonable that the strength of the 0.5h sample with large microstrains is higher than that of the 5h sample with small microstrains.

The important thing here is that both high strength and toughness are achieved through the microstructural control of stishovite so as to promote the inhomogeneous nucleation of amorphous phase. The mechanical properties will be further improved by optimizing the microstructure. Furthermore, the present results form the basis of developing strong and tough ceramics by fracture-induced amorphization: high-pressure phase the free energy of which is higher than that of amorphous phase, nanocrystalline size, large microstrain, and large dislocation density.

5. Conclusions

Strength and toughness of nanocrystalline SiO_2 stishovite,

which was toughened by fracture-induced amorphization, were investigated by using micro-cantilever beam specimens of different sizes. The results were summarized as follows:

1. The crack growth resistance curve (R-curve) rose steeply from the initial value of 4 MPa $m^{1/2}$ to 8 MPa $m^{1/2}$ with crack extension of only a few μm, and reached to a plateau value of 10.9 MPa $m^{1/2}$.
2. The strength of micro-cantilever specimens increased with decreasing the specimen size, so that the smallest specimen exhibited the highest strength of 6.3 GPa. This value gives the estimate of the lower bound of the critical stress for amorphization, which is much higher than that of martensitic transformation of zirconia.
3. The fracture toughness and strength increased with microstrain and dislocation density, which were derived during the high-pressure synthesis. The increase of strength and toughness was explained by assuming that the critical stress for amorphization was reduced by microstrain. It was also assumed that grain boundaries and dislocations acted as the sites for heterogeneous nucleation for amorphization.
4. The strength and toughness of nanocrystalline stishovite can be optimized by microstructural control, very small grain size, large microstrain, and large dislocation density, all of which promote amorphization, and decrease the critical stress. This strategy of microstructural control would be

useful to develop a wide variety of hard, strong, and tough materials by high-pressure synthesis.

Acknowledgements

This work was supported by JSPS KAKENHI Grant Number JP16K14411. The authors would like to thank Prof. Aiichiro Nakano of University of Southern California, Prof. Fuyuki Shimojo and Mr. Masaaki Misawa of Kumamoto University for discussion on amorphization. The authors warmly thank Profs. Takashi Akatsu, Yutaka Shinoda, and Ms. Risako Sekine of Tokyo Institute of Technology, Dr. Takashi Nagoshi of National Institute of Advanced Industrial Science and Technology, and Ms. Eleonora Kulik of DESY for fruitful discussions and assistance in conducting experiments.

References

[1] S.M. Stishov, S.V. Popova, New dense modifications of silica, Geochemistry 10 (1961) 923-926.

[2] J.M. Léger, J. Haines, M. Schmidt, J.P. Petitet, A.S. Pereira, J.A.H. da Jornada, Discovery of hardest known oxide, Nature 383 (1996) 401.

[3] V.V. Brazhkin, M. Grimsditch, I. Guedes, N.A. Bendeliani, T.I. Dyuzheva, L.M. Lityagina, Elastic moduli and the mechanical properties of stishovite single crystals, Phys. Usp. 45 (2002) 447-448.

[4] S.M. Wiederhorn, Fracture surface energy of glass, J. Am. Ceram. Soc. 52 (1969) 99-105.

[5] N. Nishiyama, S. Seiki, T. Hamaguchi, T. Irifune, M. Matsushita, M. Takahashi, H. Ohfuji, Y. Kono, Synthesis of nanocrystalline bulk SiO_2 stishovite with very high toughness, Scripta Mater. 67 (2012) 955-958.

[6] G.R. Anstis, P. Chantikul, B.R. Lawn, D.B. Marshall, A critical evaluation of indentation techniques for measuring fracture toughness: I, Direct crack measurements, J. Am. Ceram. Soc. 64 (1981) 533-538.

[7] P.F. Becher, Microstructural design of toughened ceramics, J. Am. Ceram. Soc. 74 (1991) 255-269.

[8] B. Mussler, M.V. Swain, N. Claussen, Dependence of fracture toughness of alumina on grain size and test technique, J. Am. Ceram. Soc. 65 (1982) 566-572.

[9] R.C. Garvie, R.H. Hannink, R.T. Pascoe, Ceramics steel?, Nature 258 (1975) 703-704.

[10] T.K. Gupta, F.F. Lange, J.H. Bechtold, Effect of stress-induced phase transformation on the properties of polycrystalline zirconia containing metastable tetragonal phase J. Mater. Sci. 13 (1978) 1464-1470.

[11] R.H. Hannink, P.M. Kelly, B.C. Muddle, Transformation toughening in zirconia-containing ceramics, J. Am. Ceram. Soc. 83 (2000) 461-487.

[12] R.M. McMeeking, A.G. Evans, Mechanics of transformation-toughening in brittle materials, J. Am. Ceram. Soc. 65 (1982) 242-246.

[13] A.G. Evans, R.M. Cannon, Toughening of brittle solids by martensttic transformations, Acta Metall. 34 (1986) 761-800.

[14] B. Budiansky, J.W. Hutchinson, J.C. Lambropoulos, Continuum theory of dilatant transformation toughening in ceramics, Int. J. Solids Structures 19 (1983) 337-355.

[15] N. Nishiyama, F. Wakai, H. Ohfuji, Y. Tamenori, H. Murata, T. Taniguchi, M. Matsushita, M. Takahashi, E. Kulik, K. Yoshida, K. Wada, J. Bednarcik, T. Irifune, Fracture-induced amorphization of polycrystalline SiO_2 stishovite: a potential platform for toughening in ceramics, Sci. Rep. 4 (2014) 6558.

[16] P. Richet, Superheating, melting and vitrification through decompression of high-pressure minerals, Nature 331 (1988) 56-58.

[17] M. Grimsditch, S. Popova, V.V. Brazhkin, R.N. Voloshin, Temperature-induced amorphization of SiO_2 stishovite, Phys. Rev. B 50 (1994) 12984-12986.

[18] A.G. Evans, Perspective on the development of high-toughness ceramics, J. Am. Ceram. Soc. 73 (1990) 187-206.

[19] D. Munz, What can we learn from R-curve measurements?, J. Am. Ceram. Soc. 90 (2007) 1-15.

[20] K. Yoshida, F. Wakai, N. Nishiyama, R. Sekine, Y. Shinoda, T. Akatsu, T. Nagoshi, M. Sone, Large increase in fracture resistance of stishovite with crack extension less than one micrometer, Sci. Rep. 5 (2015) 10993.

[21] D.B. Marshall, Strength characteristics of transformation-toughened zirconia, J. Am. Ceram. Soc. 69 (1986) 173-180.

[22] G.K. Williamson, W.H. Hall, X-ray line broadening from filed aluminium and wolfram, Acta Metall. 1 (1953) 22-31.

[23] B-N. Kim, K. Hiraga, K. Morita, H. Yoshida, T. Miyazaki, Y. Kagawa, Microstructure and optical properties of transparent alumina, Acta Mater. 57 (2009) 1319-1326.

[24] K. Takashima, Y. Higo, S. Sugiura, M. Shimojo, Fatigue crack growth behavior of micro-sized specimens prepared from an electroless plated Ni-P amorphous alloy thin film, Mater. Trans. 42 (2001) 68-73.

[25] C.F. Shih, H.G. deLorenzi, W.R. Andrews, Elastic compliances and stress-intensity factors for side-grooved compact specimens, Int. J. Fracture 13 (1977) 544-548.

[26] H.G. deLorenzi, C.D. Shih, 3-D Elastic-plastic investigation of fracture parameters in side-grooved compact specimen, Int. J. Fracture 21 (1983) 195-220.

[27] T. Namazu, Y. Isono, T. Tanaka, Evaluation of size effect on mechanical properties of single crystal silicon by nanoscale bending test using AFM, J. Microelectromech. S. 9 (2000) 450-459.

[28] J.N. Ding, Y.G. Meng, S.Z. Wen, Specimen size effect on mechanical properties of polysilicon microcantilever beams measured by deflection using a nanoindenter, Mater. Sci. Eng. B 83 (2001) 42-47.

[29] T. Klünsner, S. Wurster, P. Supancic, R. Ebner, M. Jenko, J. Glätzle, A. Püschel, R. Pippan, Effect of specimen size on the tensile strength of WC–Co hard metal, Acta Mater. 59 (2011) 4244-4252.

[30] J.J. Kruzic, R.L. Satet, M.J. Hoffmann, R.M. Cannon, R.O. Ritchie, The utility of R-curves for understanding fracture toughness-strength relations in bridging ceramics, J. Am. Ceram. Soc. 91 (2008) 1986-1994.

[31] M.V. Swain, L.R.F. Rose, Strength limitations of transformation-toughened zirconia alloys, J. Am. Ceram. Soc. 69 (1986) 511-518.

[32] E. Camposilvan, O. Torrents, M. Anglada, Small-scale mechanical behavior of zirconia, Acta Mater. 80 (2014) 239-249.

[33] M. Hemmati, A. Chizmeshya, G.H. Wolf, P.H. Poole, J. Shao, C.A. Angell, Crystalline-amorphous transition in silicate perovskites, Phys. Rev. B 51 (1995) 14841-14848.

[34] S. Karato, K. Fujino, E. Ito, Plasticity of $MgSiO_3$ perovskite: The results of microhardness tests on single crystals, Geophys. Res. Lett. 17 (1990) 13-16.

[35] X. Xue, J.F. Stebbins, M. Kanzaki, A ^{29}Si MAS NMR Study of sub-T_g amorphization of stishovite at ambient pressure, Phys. Chem. Minerals 19 (1993) 480-485.

[36] V.V. Brazhkin, R.N. Voloshin, S.V. Popova, The kinetics of the transition of the metastable phases of SiO_2, stishovite and coesite to the amorphous state, J. Non-Cryst. Solids 136 (1991) 241-248.

[37] J.R. Patel, M. Cohen, Criterion for the action of applied stress in the martensitic transformation, Acta Metall. 1 (1953) 531-538.

[38] S-N. Luo, L. Zheng, O. Tschauner, Spontaneous disordering of nm-grain-sized polycrystals and clusters of silica stishovite, Solid State Comm. 136 (2005) 71-75.

[39] S-N. Luo, L. Zheng, O. Tschauner, Solid-state disordering and melting of silica stishovite: the role of defects, J. Phys.: Condens. Matter. 18 (2006) 659-668.

[40] M. Sugiyama, S. Endo, K. Koto, The crystal structure of stishovite under pressure up to 6 GPa, Mineral. J. 13 (1987) 455-466.

[41] P. Cordier, T.G. Sharp, Large angle convergent beam electron diffraction determinations of dislocation Burgers vectors in synthetic stishovite, Phys. Chem. Minerals 25 (1998) 548-555.

Figure Captions

Fig. 1. R-curve testing by using a notched micro-cantilever specimen. (a) Geometry of the specimen, (b) side view of the notch, (c) notch tip, (d) top view of side-grooves, (e) ion beam directions during FIB machining.

Fig. 2. Specimen geometry and fracture surface of (a) specimen without side grooves and (b) specimen with side-grooves. The crack curved toward the fixed end in the specimen without side grooves, but the crack propagation is macroscopically flat in the specimen with side-groove.

Fig. 3. TEM images of microstructure of nano-crystalline stishovite samples. (a) 0.5h sample (average grain size: 128 nm, microstrain: 0.34 %), (b) 5h sample (average grain size: 164 nm, microstrain: 0.24 %)

Fig. 4. Microstrain as a function of synthesis temperature. The microstrain decreases with decreasing synthesis temperature. At the same synthesis temperature, microstrain decreases with increasing the holding time.

Fig. 5. Micro-mechanical testing of notched specimens of different sizes for the 0.5h sample. (a) Load-displacement curves ($P-u$ curves). (b) R-curve behavior.

Fig. 6. Comparison between R-curves of the 0.5h sample and that of the 5h sample. The plateau value of the 0.5h sample with large microstrain is higher than that of the 5h sample with small microstrain.

Fig. 7. Strength of nanocrystalline stishovite plotted as a function of the volume of micro-sized specimens. Strengths of alumina, zirconia, silica glass, and single crystal of silicon are also plotted for comparison.

Fig. 8. Relationship between fracture strength and critical transformation stress σ_c. The strength is limited by fracture toughness in the failure from pre-existing flaw region. The strength is limited by σ_c in the yield limited region. The strength of stishovite is higher than that of zirconia which is limited by σ_c of 3 GPa. As σ_c is reduced by the presence of microstrain, fracture toughness and strength are increased with microstrain.

Fig. 9. Energy diagram of amorphization of stishovite. Applied tensile stress reduces the height of the energy barrier. The presence of microstrain further reduces the energy barrier, and decreases the critical stress.

Table 1. Dimensions of micro-cantilever specimens

Material	Specimen	H [μm]	B [μm]	B_N [μm]	W [μm]	L [μm]	a_0 [μm]
0.5h sample	W20	20.1	18.0	14.9	19.7	60.6	9.64
		19.8	18.4	15.0	20.8	60.6	8.24
	W40	40.5	33.2	24.7	44.5	119.8	22.0
	W60	54.9	51.7	40.5	61.7	179.2	30.5

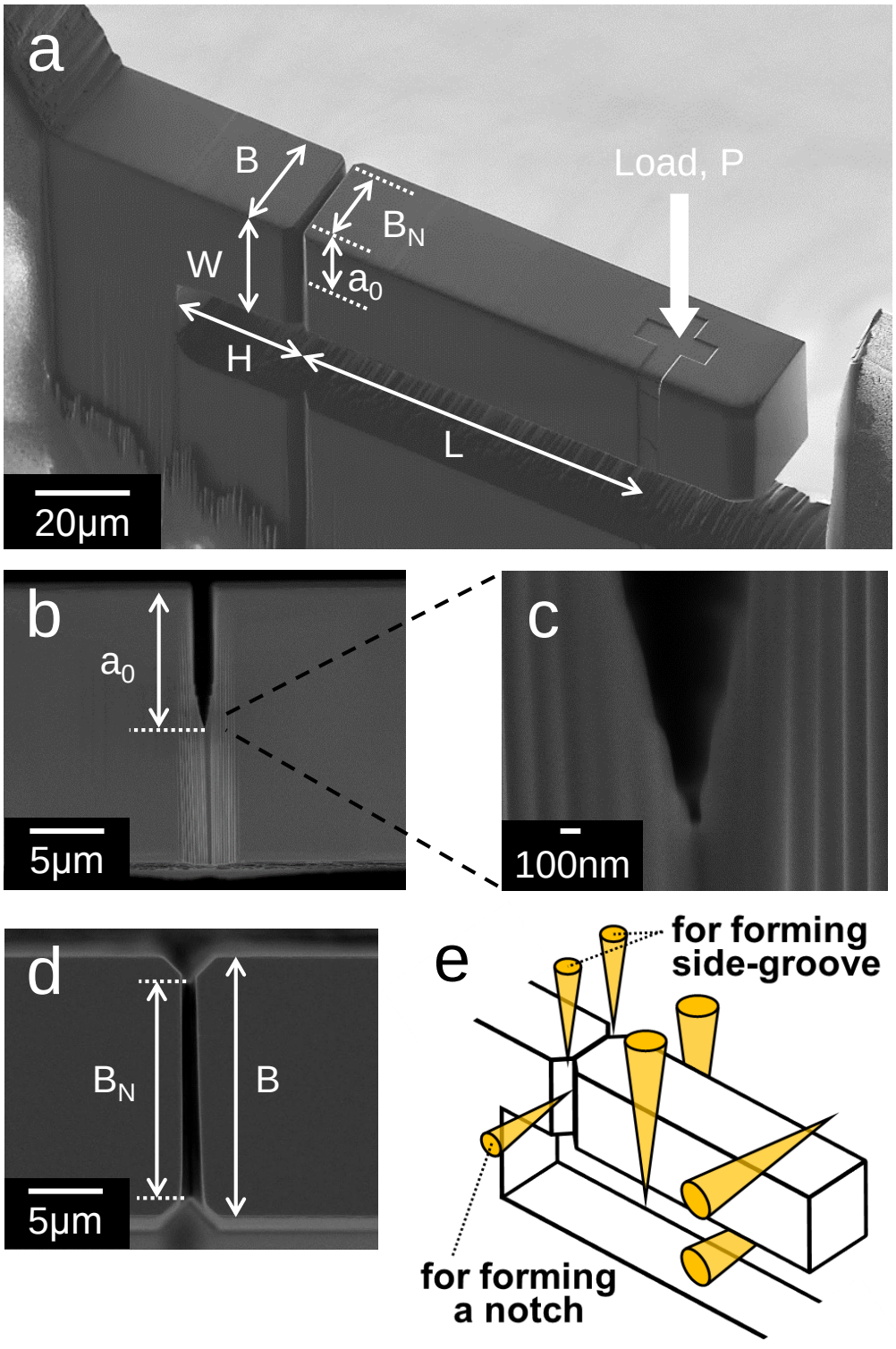

Fig. 1. R-curve testing by using a notched micro-cantilever specimen. (a) Geometry of the specimen, (b) side view of the notch, (c) notch tip, (d) top view of side-grooves, (e) ion beam directions during FIB machining.

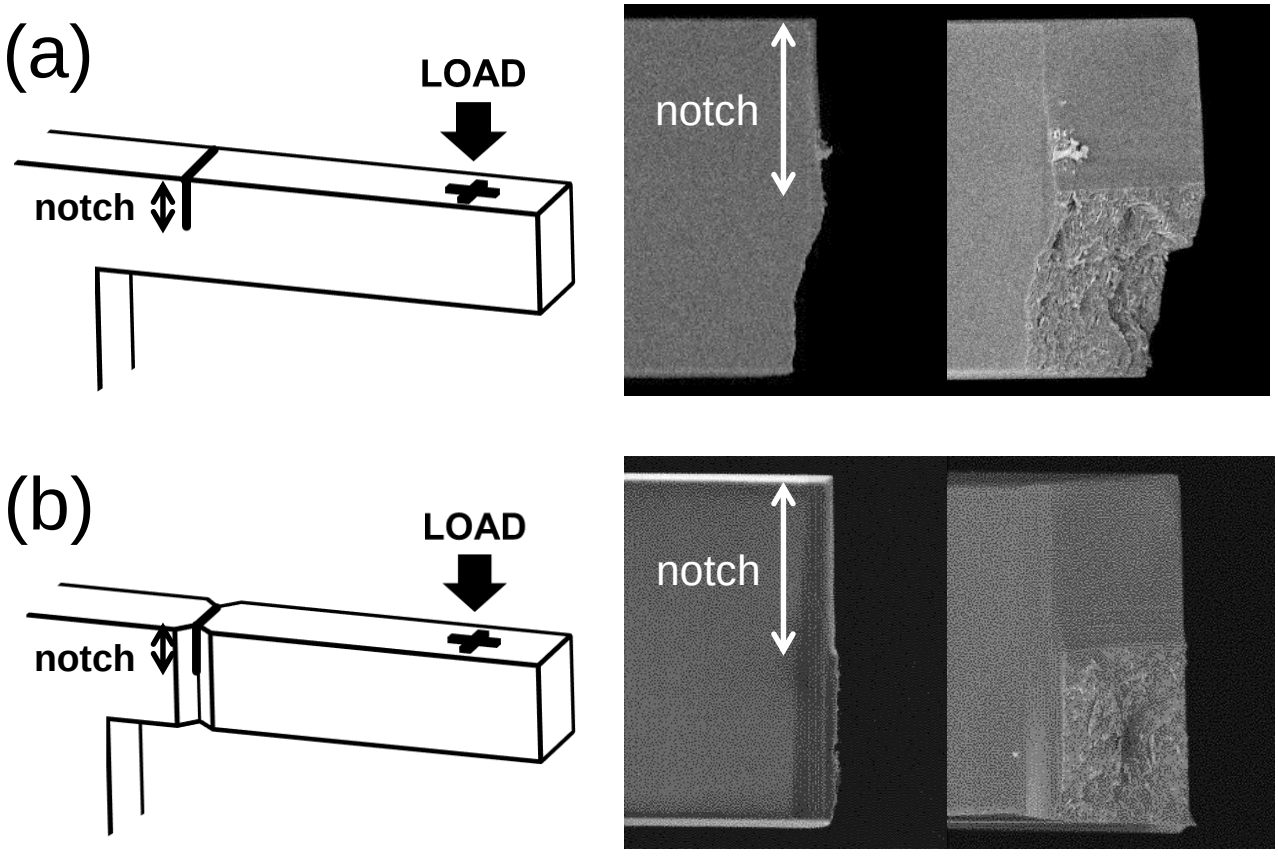

Fig. 2. Specimen geometry and fracture surface of (a) specimen without side grooves and (b) specimen with side-grooves. The crack curved toward the fixed end in the specimen without side grooves, but the crack propagation is macroscopically flat in the specimen with side-groove.

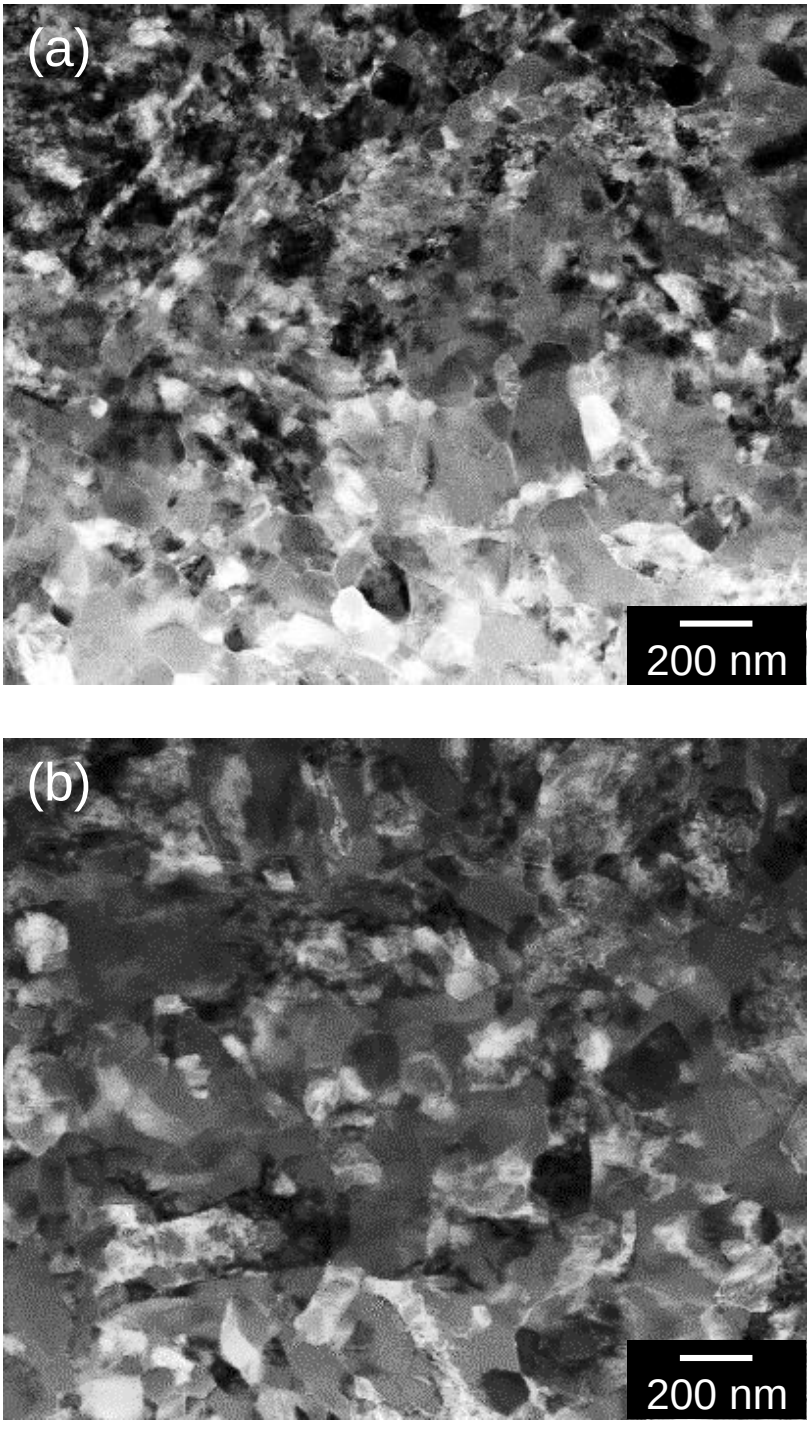

Fig. 3. TEM images of microstructure of nano-crystalline stishovite samples. (a) 0.5h sample. (average grain size: 128 nm, microstrain: 0.34%) (b) 5h sample. (average grain size: 164 nm, microstrain: 0.24%)

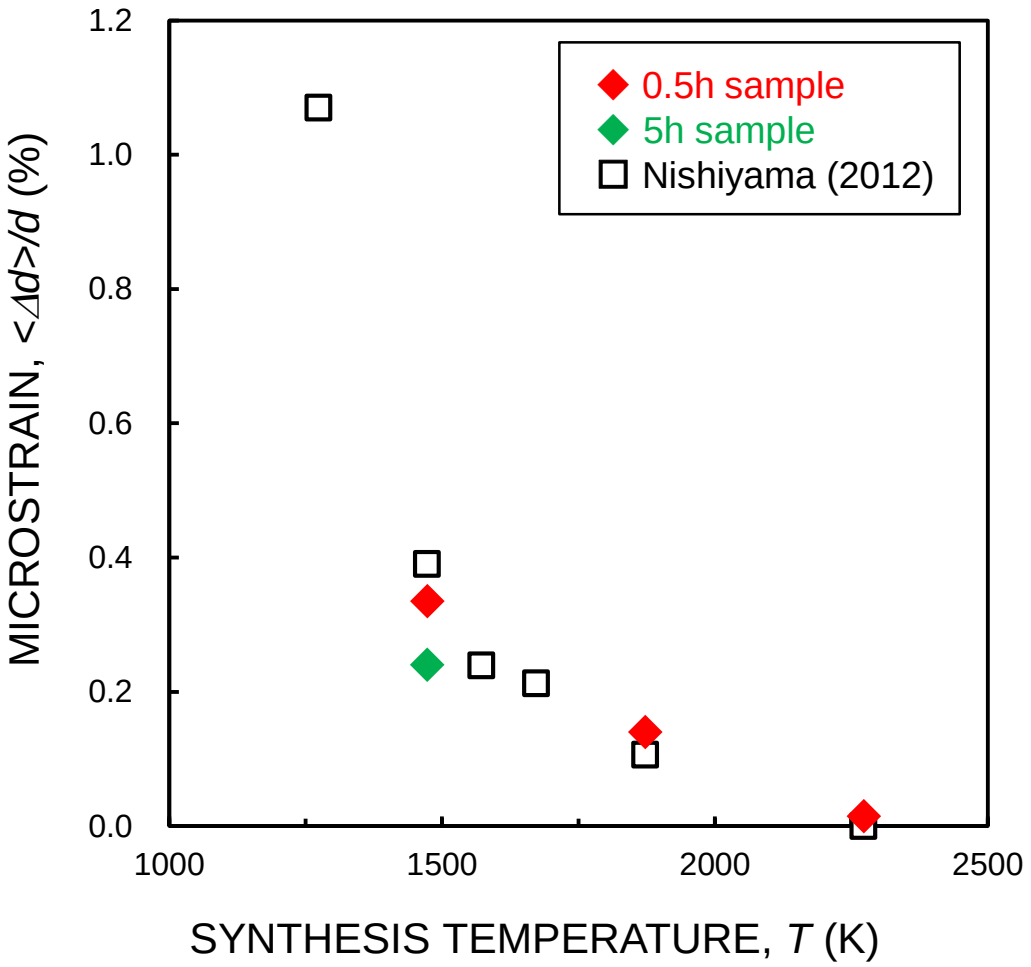

Fig. 4. Microstrain as a function of synthesis temperature. The microstrain decreases with decreasing synthesis temperature. At the same synthesis temperature, microstrain decreases with increasing the holding time.

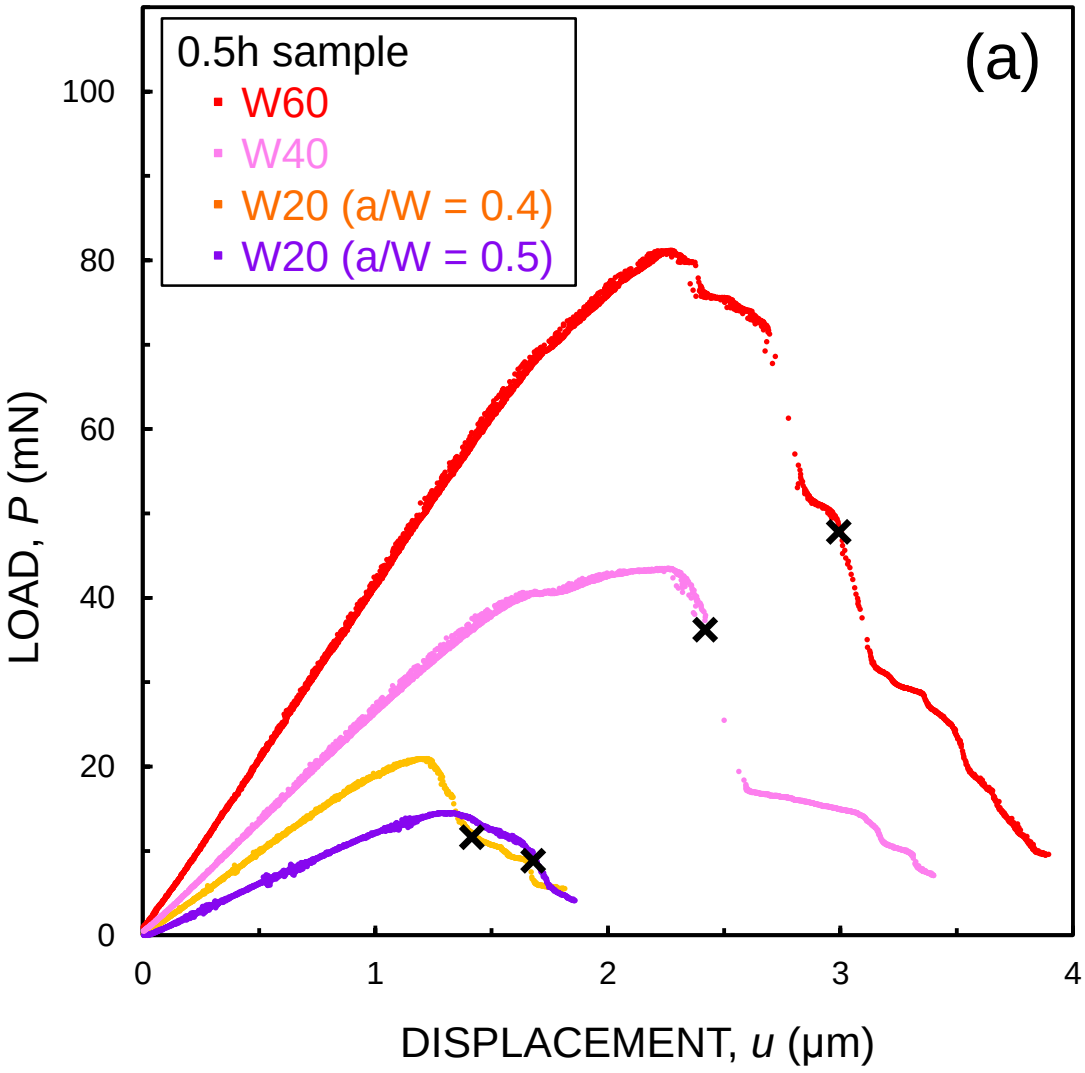

Fig. 5. Micro-mechanical testing of notched specimens of different sizes for the 0.5h sample. (a) Load-displacement curves (P-u curves).

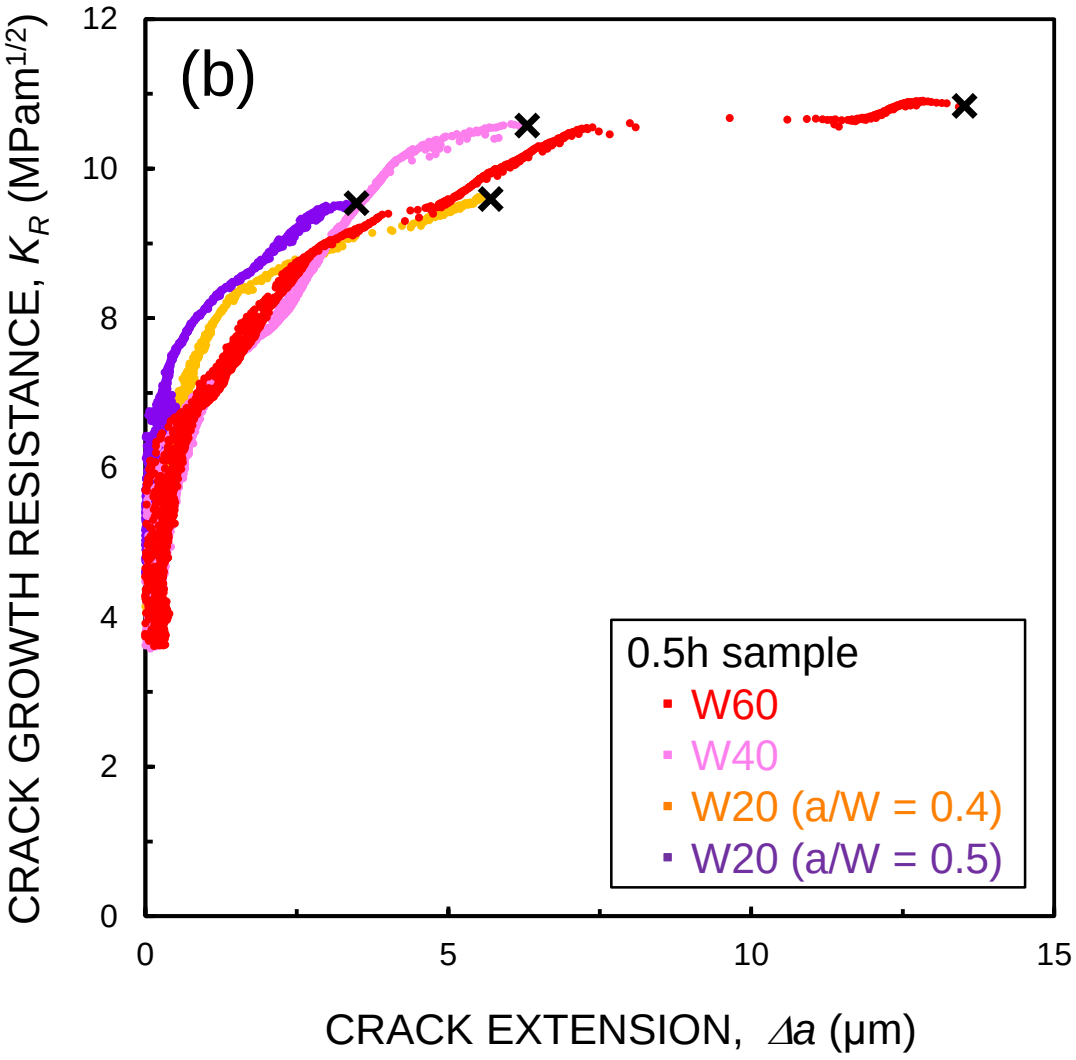

Fig. 5. Micro-mechanical testing of notched specimens of different sizes for the 0.5h sample. (b) R-curve behavior.

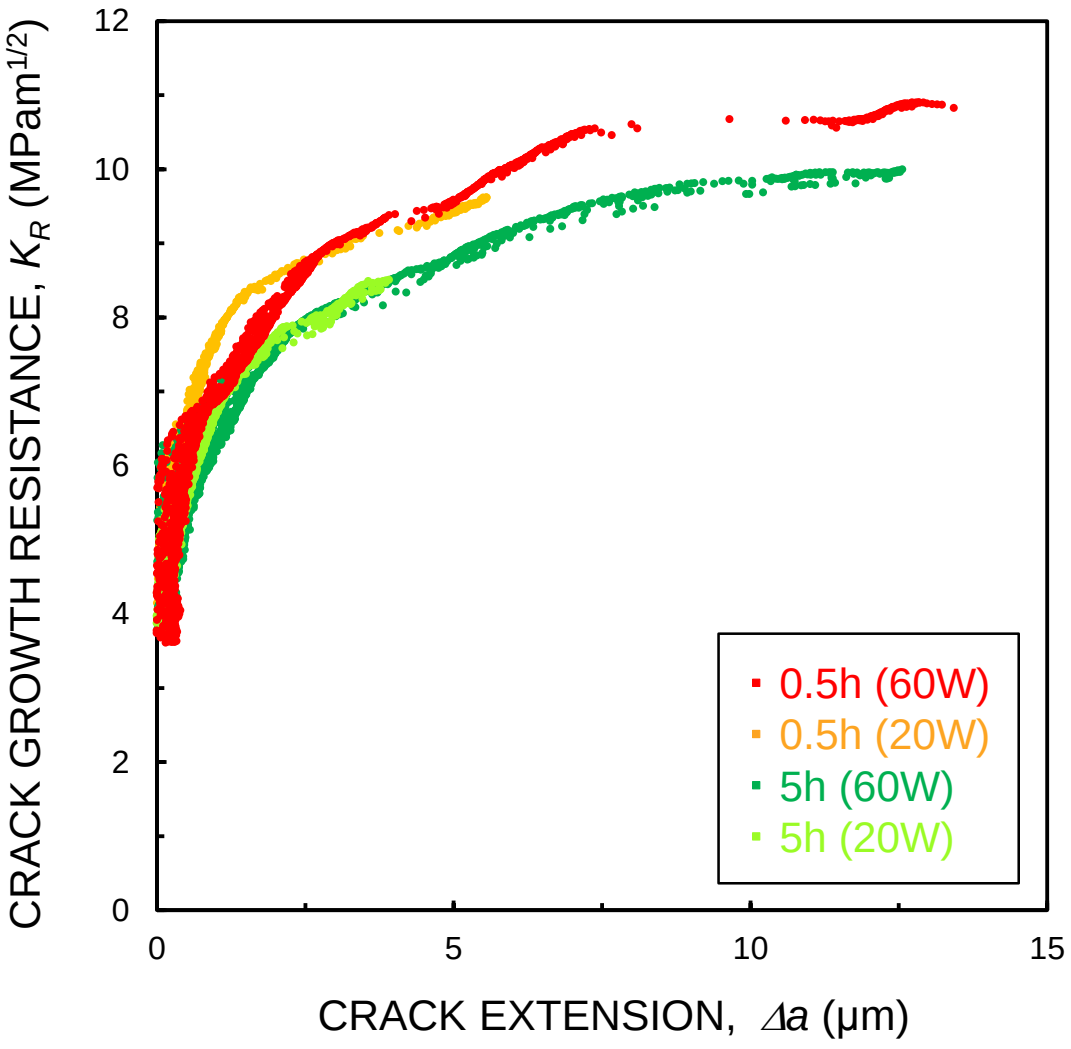

Fig. 6. Comparison between R-curves of the 0.5h sample and that of the 5h sample. The plateau value of the 0.5h sample with large microstrain, is higher than that of the 5h sample with small microstrain.

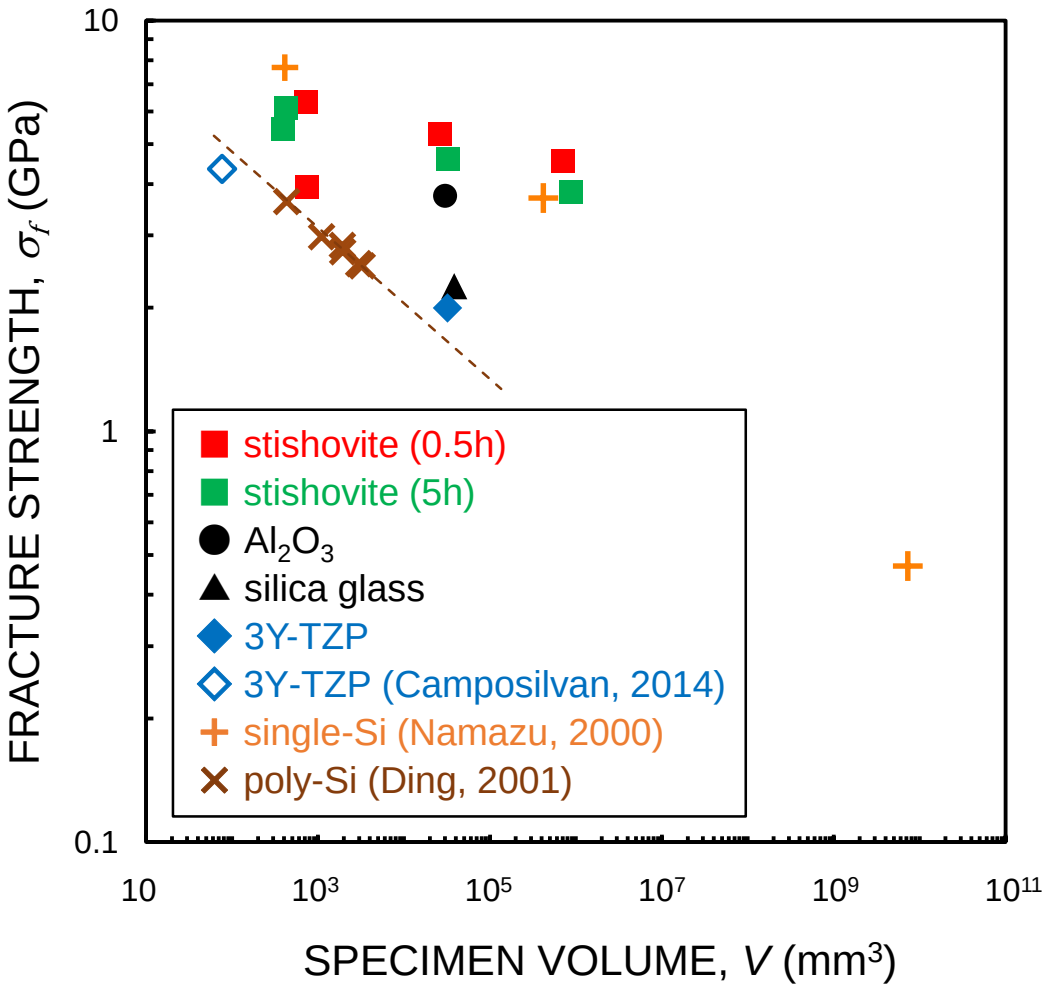

Fig. 7. Strength of nanocrystalline stishovite plotted as a function of the volume of micro-sized specimens. Strengths of alumina, zirconia, silica glass, and single crystal of silicon are also plotted for comparison.

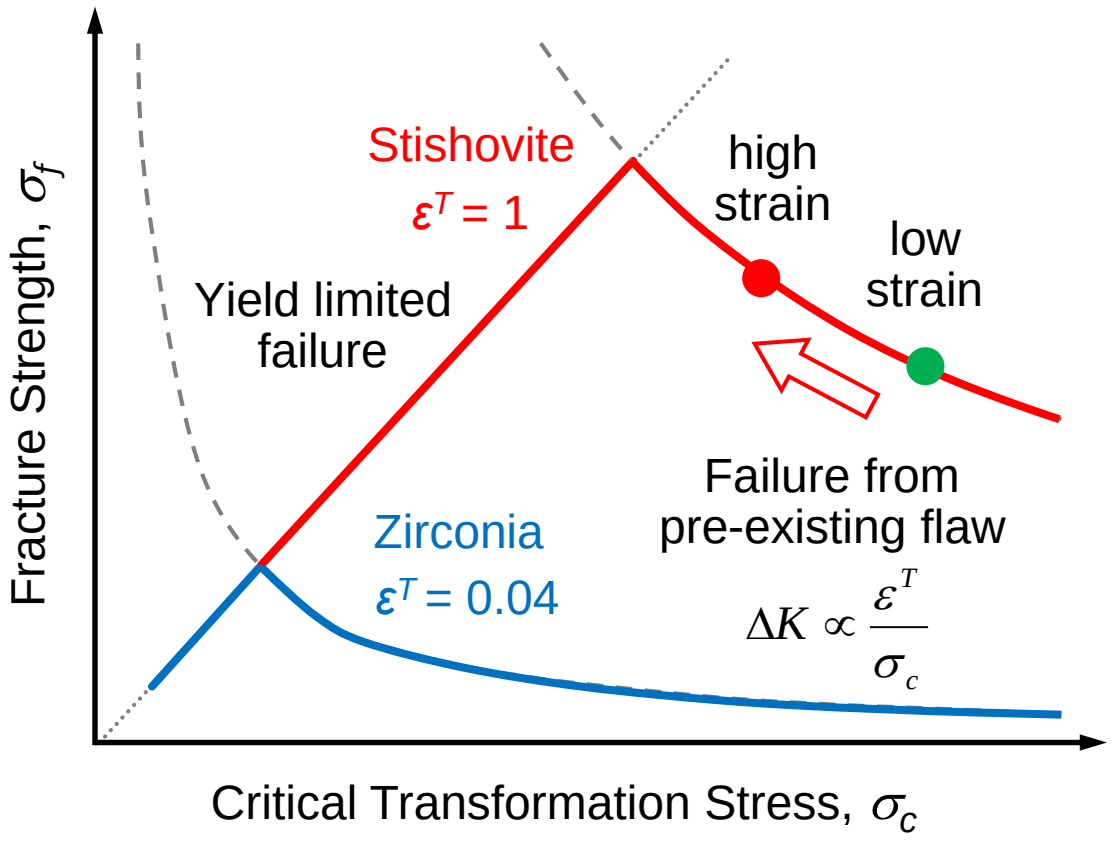

Fig. 8. Relationship between fracture strength and critical transformation stress σ_c. The strength is limited by fracture toughness in the failure from pre-existing flaw region. The strength is limited by σ_c in the yield limited region. The strength of stishovite is higher than that of zirconia which is limited by σ_c of 3 GPa. As σ_c is reduced by the presence of microstrain, fracture toughness and strength are increased with microstrain.

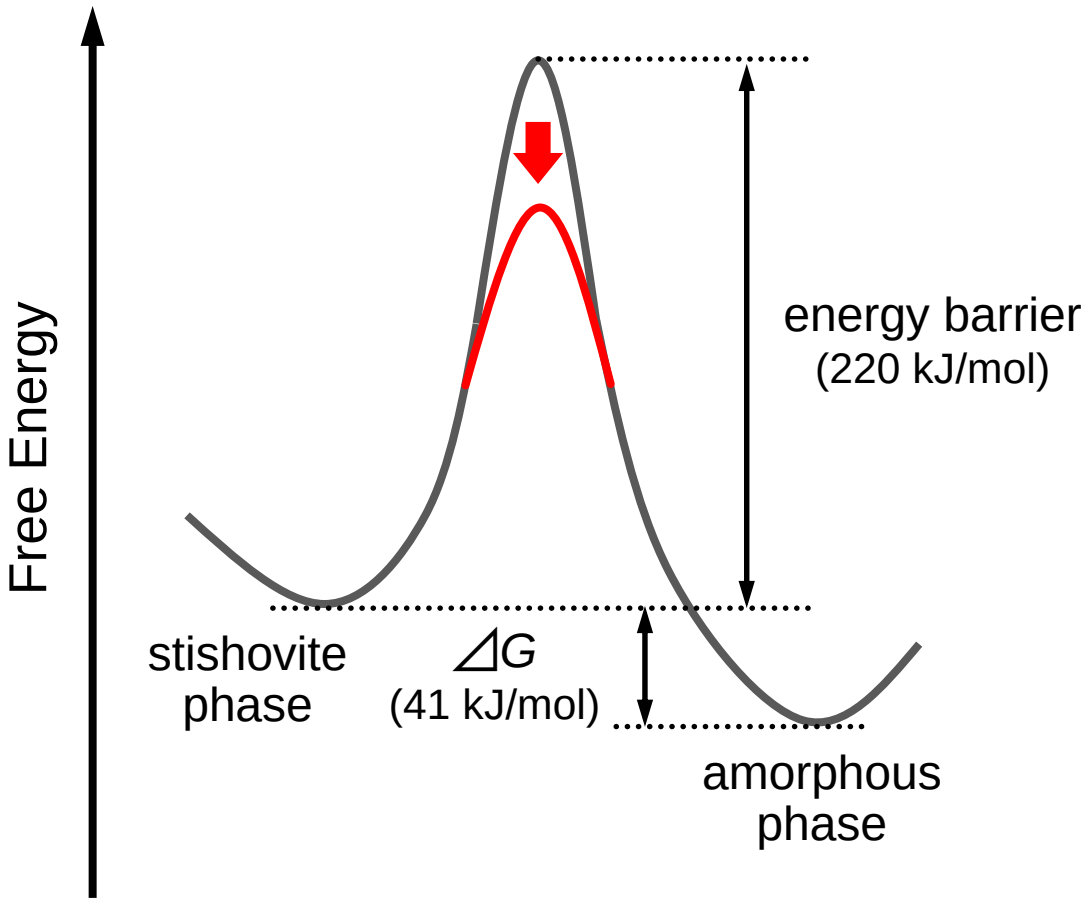

Fig. 9. Energy diagram of amorphization of stishovite. Applied tensile stress reduces the height of the energy barrier. The presence of microstrain further reduces the energy barrier, and decreases the critical stress.